



Detecting obstructive coronary artery disease with machine learning: rest-only gated single photon emission computed tomography myocardial perfusion imaging combined with coronary artery calcium score and cardiovascular risk factors

Bao Liu^{1,2}, Wenji Yu^{1,2}, Feifei Zhang^{1,2}, Yunmei Shi^{1,2}, Le Yang^{1,2}, Qi Jiang^{1,2}, Yufeng Wang^{1,2}, Yuetao Wang^{1,2}[^]

¹Department of Nuclear Medicine, The Third Affiliated Hospital of Soochow University, Changzhou, China; ²The Nuclear Medicine and Molecular Imaging Clinical Translation Institute of Soochow University, Changzhou, China

Contributions: (I) Conception and design: YT Wang; (II) Administrative support: YT Wang, B Liu; (III) Provision of study materials or patients: W Yu, F Zhang; (IV) Collection and assembly of data: Y Shi, L Yang; (V) Data analysis and interpretation: Q Jiang, YF Wang; (VI) Manuscript writing: All authors; (VII) Final approval of manuscript: All authors.

Correspondence to: Yuetao Wang. Department of Nuclear Medicine, The Third Affiliated Hospital of Soochow University, 185 Juqian Street, Changzhou 213003, China. Email: yuetao-w@163.com.

Background: The rest-only single photon emission computed tomography (SPECT) myocardial perfusion imaging (MPI) has low diagnostic performance for obstructive coronary artery disease (CAD). Coronary artery calcium score (CACS) is strongly associated with obstructive CAD. The aim of this study was to investigate the performance of rest-only gated SPECT MPI combined with CACS and cardiovascular risk factors in diagnosing obstructive CAD through machine learning (ML).

Methods: We enrolled 253 suspected CAD patients who underwent the 1-stop rest-only SPECT MPI and computed tomography (CT) scan due to stress test-related contraindications. Myocardial perfusion and wall motion were assessed using quantitative perfusion SPECT + quantitative gated SPECT (QPS + QGS) automated quantification software. The Agatston algorithm was used to calculate CACS. The clinical data of patients, including cardiovascular risk factors, were collected. Based on feature selection and clinical experience, 8 factors were identified as modeling variables. Subsequently, patients were divided randomly into 2 groups: the training (70%) and test (30%) groups. The performance of 8 supervised ML algorithms was evaluated in the training and test groups.

Results: Obstructive CAD was diagnosed by coronary angiography in 94 (37.2%, 94/253) patients. In the training group, the area under the receiver operator characteristic (ROC) curve (AUC) of the random forest was the highest, and the AUCs of Logistic, extreme gradient boosting (XGBoost), support vector machine (SVM), and adaptive boosting (AdaBoost) were all above 0.9. In the test group, the AUC of recursive partitioning and regression trees (Rpart) was the highest (0.911). Rpart and Naïve Bayes had the highest accuracy (0.840). Rpart had a sensitivity and specificity of 0.851 and 0.821, respectively; Naïve Bayes had a sensitivity and specificity of 0.809 and 0.893, respectively. Next was Logistic, with an accuracy of 0.827, a sensitivity of 0.872, and a specificity of 0.750. The random forest and XGBoost algorithms also had high accuracy, which was 0.813 for each algorithm.

Conclusions: Rest-only SPECT MPI combined with CACS and cardiovascular risk factors using an ML algorithm to detect obstructive CAD is feasible. Among the algorithms validated in the test group, Rpart,

[^] ORCID: 0000-0003-2859-8625.

Naïve Bayes, XGBoost, Logistic, and random forest are all highly accurate for diagnosing obstructive CAD. The application of ML in resting MPI and CACS may be used for screening obstructive CAD.

Keywords: Machine learning (ML); myocardial perfusion imaging (MPI); single photon emission computed tomography (SPECT); coronary artery calcium score (CACS); coronary artery disease (CAD)

Submitted Jul 21, 2022. Accepted for publication Dec 08, 2022. Published online Feb 06, 2023.

doi: 10.21037/qims-22-758

View this article at: <https://dx.doi.org/10.21037/qims-22-758>

Introduction

Currently, the global population continues to bear the enormous burden of coronary artery disease (CAD). Gated single photon emission computed tomography (SPECT) myocardial perfusion imaging (MPI) is a widely used noninvasive method for diagnosing CAD (1,2). SPECT MPI can show the location, extent, and severity of myocardial ischemia or infarction and provide information on myocardial perfusion and global and regional function (3-5). Nonetheless, the results of SPECT MPI may be incorrectly negative in patients with multivessel CAD, particularly those with 3-vessel diffuse illness, due to “balanced ischemia”, resulting in a missed diagnosis of severe CAD (6-8). At the same time, obstructive CAD increases with coronary artery calcium score (CACS), which reflects the burden of coronary atherosclerotic plaque (9,10). Previous research has shown that adding CACS to stress MPI improves the diagnosis of CAD (11).

Artificial intelligence (AI) is a growing and powerful technology in healthcare. In recent years, the application of AI in nuclear cardiology has become increasingly extensive (12-17). An interpretable algorithm based on deep learning was used to diagnose obstructive CAD in stress or stress/rest MPI (15,18). However, stress MPI is not suitable for all patients, as stress tests are contraindicated in patients with suspected acute coronary syndrome (ACS) (19). Previous studies found that, despite the addition of wall motion, rest-only MPI had limited value in detecting CAD, with a sensitivity of less than 50% (20,21). To date, there have been no studies of resting MPI combined with CACS and cardiovascular risk factors using machine learning (ML) to detect obstructive CAD. Therefore, the purpose of this study was to use ML to evaluate the value of rest-only MPI combined with CACS and cardiovascular risk factors for detecting obstructive CAD in suspected CAD patients. We present the following article in accordance with the TRIPOD reporting checklist (available at <https://qims.amegroups.com/article/view/10.21037/qims-22-758/rc>).

[amegroups.com/article/view/10.21037/qims-22-758/rc](https://qims.amegroups.com/article/view/10.21037/qims-22-758/rc).

Methods

Study cohort and population

We recruited a retrospective cohort of suspected CAD patients who underwent gated SPECT MPI at the Third Affiliated Hospital of Soochow University from February 2016 to April 2020. The following were the inclusion criteria: (I) no history of a definite myocardial infarction, (II) a contraindication to stress test, (III) no history of percutaneous coronary intervention (PCI) or coronary artery bypass grafting (CABG), and (IV) coronary angiography was completed within 3 months of the examination. Severe valvular disease, hypertrophic or dilated cardiomyopathy, severe arrhythmias, poor image quality due to motion artifacts, and a lack of CACS scan data were the exclusion criteria. Finally, 253 patients were included in the study, including 61 with suspected ACS, 39 with decompensated heart failure, 41 with bradycardia combined with restricted physical activity, 54 with uncontrolled hypertension (systolic blood pressure >200 mmHg), and 58 with asthma. The detailed process of patient recruitment and study design is shown in *Figure 1*. The Ethics Committee of the Third Affiliated Hospital of Soochow University approved the research protocol, which complied with the Declaration of Helsinki (as revised in 2013). The requirement for informed consent was waived since the study was retrospective.

Resting image acquisition and analysis

^{99m}Tc-sestamibi (^{99m}Tc-MIBI) (740–925 MBq) was administered intravenously at rest. Scanning was started after 60–90 min of rest. A dual-head 90° gamma camera (Symbia T16; Siemens Medical Systems, Erlangen, Germany) equipped with a parallel-hole collimator with low energy and high resolution was used for image acquisition.

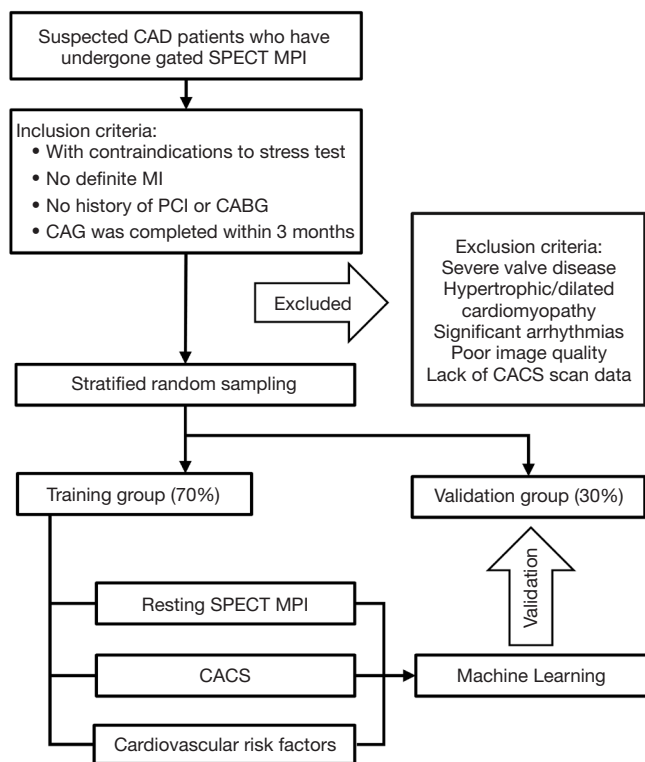


Figure 1 Flowchart of patient recruitment and study design. CAD, coronary artery disease; SPECT, single photon emission computerized tomography; MPI, myocardial perfusion imaging; MI, myocardial infarction; PCI, percutaneous coronary intervention; CABG, coronary artery bypass grafting; CAG, coronary angiography; CACS, coronary artery calcium score.

Detailed scan parameters are provided in our previous study (22). All SPECT image acquisition procedures followed the recommendations of the relevant guidelines (23). Perfusion images were analyzed using an international 17-segment model (24), which was divided into territories of the left anterior descending coronary artery (LAD), left circumflex coronary artery (LCX), and right coronary artery (RCA). Quantitative perfusion SPECT + quantitative gated SPECT (QPS + QGS) 2009 automated analysis software (Cedars-Sinai Medical Center, Los Angeles, CA, USA) were used for semi-quantification of perfusion and wall motion, which scored perfusion (0–4) and wall motion (0–5) according to the degree of abnormality. The detailed meaning of the scores can be found in the relevant studies (25,26). Quantitative analysis of images was performed by a nuclear cardiologist. The summed rest score (SRS) or summed motion score (SMS) was the sum of

the 17-segment resting perfusion or wall motion scores. An $SRS \geq 4$ or $SMS \geq 2$ exhibited in 2 consecutive segments in 1 territory was considered abnormal (20,25).

CACS acquisition and analysis

A chest CT for obtaining CACS was performed after the completion of the MPI acquisition. Scan details were as follows: tube voltage, 120 kV; tube current, 100 mA; thickness, 3 mm; 60–80% of the R-R interval, and completed with 1 breath-hold after inhalation. The scanning range was from the plane below the tracheal carina to 1–2 cm below the heart's diaphragmatic surface. Coronary artery calcifications were identified as dense areas in coronary arteries that exceeded the 130 Hounsfield unit (HU) threshold using the Agatston algorithm (27). CACS was measured independently by a nuclear cardiologist. The sum of the calcium scores of left main coronary artery (LM), LAD, LCX, RCA, and their branches was defined as CACS, and then CACS was divided into 4 categories: 0, 1–100, 101–399, and ≥ 400 (28,29).

Invasive coronary angiography

All coronary angiograms were visually interpreted on-site by 2 cardiologists. Obstructive CAD was defined as $\geq 70\%$ narrowing of the inner diameter of the LAD, LCX, RCA, or their main branches and $\geq 50\%$ narrowing of the LM (30). If 2 physicians disagreed on the results, a third senior physician was invited to read the angiograms, and the final decision was the opinion with the most votes.

ML techniques

We performed feature selection based on clinical experience and actual situations before ML. Combining variable selection from our previous study (22) and clinical experience, we finally identified the following 8 variables: age, gender, hypertension, diabetes, hyperlipidemia, SRS, SMS, and CACS. The correlation between variables was analyzed using Spearman correlation (R package: corrplot). The study population included 253 suspected CAD patients who underwent rest-only MPI due to stress contraindications. Participants were divided at random into 2 groups: the training (70%) and test (30%) groups. We selected supervised ML algorithms developed in R statistical software (version 4.1.0, R Foundation for Statistical Computing, Vienna, Austria). A total of 8 ML

Table 1 Clinical characteristics of the 253 suspected CAD patients

Variables	Without obstructive CAD (n=159)	With obstructive CAD (n=94)	P value
Age (years old)	60.9±9.3	62.7±9.0	0.131
Male	97 (61.0)	72 (76.6)	0.011
BMI (kg/m ²)	25.0±3.0	24.6±3.0	0.307
Hypertension	102 (64.2)	72 (76.6)	0.039
Diabetes	26 (16.4)	35 (37.2)	<0.001
Hyperlipidemia	92 (57.9)	74 (78.7)	0.001
Smoking >1 year	58 (36.5)	41 (43.6)	0.261
Medical treatment			
ACEI	81 (50.9)	58 (61.7)	0.097
Beta-blockers	98 (61.6)	66 (70.2)	0.167
Calcium channel blockers	95 (59.7)	54 (57.4)	0.719

Data are shown as mean ± standard deviation or number (percentage). CAD, coronary artery disease; BMI, body mass index; ACEI, angiotensin-converting enzyme inhibitor.

algorithms were used: Logistic (31), recursive partitioning and regression trees (Rpart) (R package: rpart), random forest (32), extreme gradient boosting (XGBoost) (R package: xgboost), Naïve Bayes (R package: naivebayes), K-nearest neighbor (KNN) (R package: kknn), support vector machine (SVM) (R package: e1071), and adaptive boosting (AdaBoost) (33). Except for tree-based ML algorithms, we performed feature normalization. We used a 10-fold cross-validation approach, conducted twice, for the training data. We tuned the free parameters for each algorithm using this subset. For both the training and test groups, we computed accuracy, sensitivity, specificity, positive predictive value (PPV), negative predictive value (NPV), and the area under the receiver operator characteristic curve (AUC).

Statistical methods

All statistical analysis was performed using the R software. Continuous variables that conformed to the normal distribution were expressed as the mean ± SD, and continuous variables that did not conform to the normal distribution were expressed as the median P50 (P25, P75). Chi-square tests were used for categorical variable comparisons between groups. The unpaired *t*-test for normal continuous variables or Mann–Whitney U test for skewed continuous variables were used for comparisons between 2 groups. The receiver operator characteristic

curve (ROC) analysis was used to assess the discrimination of models. The best cutoff value was calculated using Youden index. A 2-sided P value less than 0.05 was considered statistically significant.

Results

Among 253 patients with suspected CAD, 94 (37.2%, 94/253) were diagnosed with obstructive CAD by coronary angiography. Participants were divided randomly into 2 groups: the training (70%, n=178) and test (30%, n=75) groups. A total of 8 ML algorithms were used and validated, with detailed results presented below.

Demographics and clinical characteristics

The mean age was 62.7±9.0 years in the obstructive CAD group and 60.9±9.3 years in the nonobstructive CAD group (P=0.131). There was a higher proportion of males in the obstructive CAD group compared with the nonobstructive CAD group (76.6% vs. 61.0%; P=0.011). There were no significant differences in body mass index (BMI) and smoking history between the 2 groups. Cardiovascular risk factors, including hypertension, diabetes, and hyperlipidemia, were more prevalent in patients with obstructive CAD. There was no significant difference in medication history, such as angiotensin-converting enzyme inhibitors, beta-blockers, or calcium channel blockers,

Table 2 The SPECT MPI variables and CACS in 253 suspected CAD patients

Variables	Without obstructive CAD (n=159)	With obstructive CAD (n=94)	P value
Gated SPECT			
EDV (mL)	83.0 (67.0–105.0)	89.0 (71.0–114.3)	0.075
ESV (mL)	30.0 (21.0–41.0)	33.5 (25.8–48.3)	0.003
LVEF (%)	65.4±8.7	58.3±12.4	<0.001
SRS	0.0 (0.0–1.0)	2.0 (0.0–7.0)	<0.001
SMS	0.0 (0.0–0.0)	1.0 (0.0–9.3)	<0.001
PFR	2.3±0.5	2.1±0.6	0.001
CACS	0.0 (0.0–9.1)	152.9 (47.7–442.5)	<0.001
CACS: 0 (%)	111 (69.8)	12 (12.8)	<0.001
CACS: 1–100 (%)	33 (20.8)	21 (22.3)	0.766
CACS: 101–399 (%)	11 (6.9)	36 (38.3)	<0.001
CACS ≥400 (%)	4 (2.5)	25 (26.6)	<0.001

Data are shown as mean ± standard deviation, median (interquartile range) or number (percentage). SPECT, single photon emission computerized tomography; MPI, myocardial perfusion imaging; CACS, coronary artery calcium score; CAD, coronary artery disease; EDV, end diastolic volume; ESV, end systolic volume; LVEF, left ventricular ejection fraction; SRS, summed rest score; SMS, summed motion score; PFR, peak filling rate.

between the 2 groups. The clinical characteristics are displayed in *Table 1*.

Characteristics of gated SPECT MPI and CACS

Participants with obstructive CAD had lower left ventricular ejection fraction (LVEF) and a peak filling rate (PFR) compared to the group without obstructive CAD. End-diastolic volume (EDV), end-systolic volume (ESV), SRS, and SMS were higher in the obstructive CAD group than in the nonobstructive CAD group. In the group without obstructive CAD, 111 (69.8%, 111/159) patients had a CACS of 0 and 33 (20.8%, 33/159) had a CACS between 1 and 100. In the obstructive CAD group, 36 (38.3%, 36/94) patients had a CACS between 101 and 399, and 25 (26.6%, 25/94) had a CACS ≥400. The characteristics of gated SPECT MPI and CACS are displayed in *Table 2*. *Figure 2* shows the distribution and probability density of continuous variables in patient characteristics.

Diagnostic efficacy of 8 ML algorithms for predicting obstructive CAD in the training group

The Spearman correlation coefficients of the included features were calculated (*Figure 3*). Most features had

weak correlations with absolute values less than 0.25. The correlation between SMS and SRS was moderate ($\rho=0.58$) and was the highest correlation among the features. The lower correlation values shown by the heatmap indicated the absence of redundant features.

As shown in *Figure 4*, The AUCs of Logistic, Rpart, random forest, XGBoost, Naïve Bayes, KNN, SVM, and AdaBoost in the training group were 0.905 [95% confidence interval (CI): 0.861–0.949], 0.893 (95% CI: 0.841–0.944), 1.000 (95% CI: 1.000–1.000), 0.922 (95% CI: 0.878–0.965), 0.897 (95% CI: 0.853–0.942), 0.874 (95% CI: 0.819–0.929), 0.925 (95% CI: 0.883–0.967), and 0.953 (95% CI: 0.926–0.979), respectively. The AUC of the random forest was the highest, and the AUCs of Logistic, XGBoost, SVM, and AdaBoost were all above 0.9. The accuracy, sensitivity, specificity, PPV, and NPV of each algorithm for diagnosing obstructive CAD are shown in *Table 3* and *Figure 5*. Random forest, SVM, AdaBoost, and XGBoost techniques exhibited high accuracy, although each had advantages in terms of sensitivity or specificity.

Diagnostic efficacy of ML algorithms in the test group

The AUCs of Logistic, Rpart, random forest, XGBoost, Naïve Bayes, KNN, SVM, and AdaBoost in the test

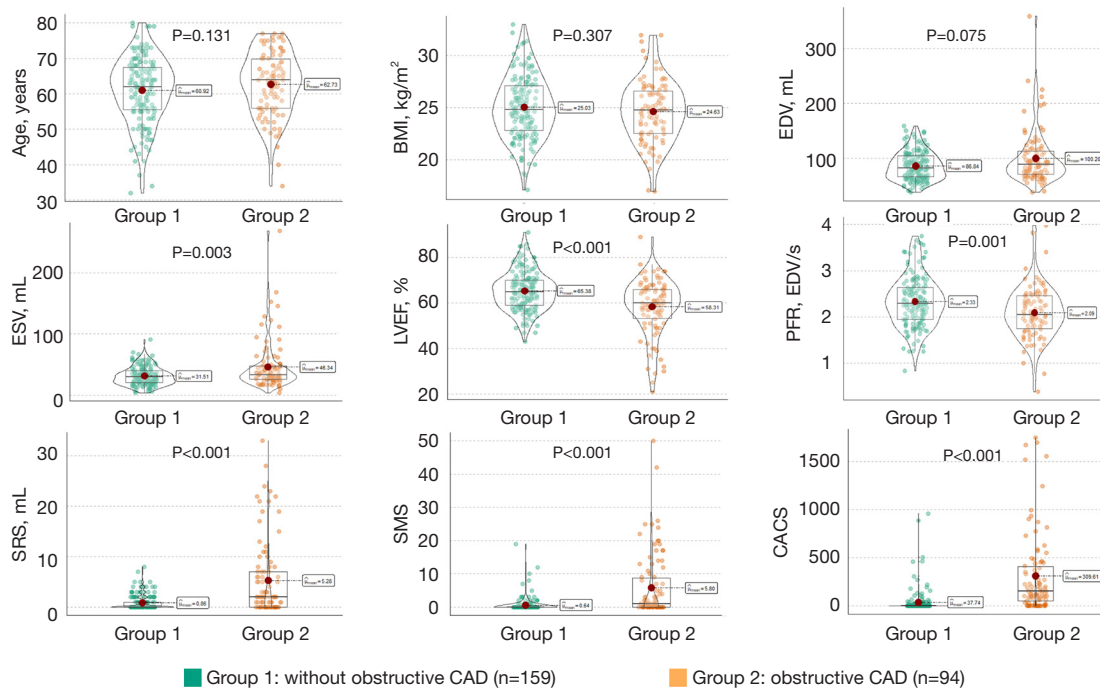


Figure 2 Violin plot comparing characteristics of patients between groups. BMI, body mass index; EDV, end diastolic volume; ESV, end systolic volume; LVEF, left ventricular ejection fraction; PFR, peak filling rate; SRS, summed rest score; SMS, summed motion score; CACS, coronary artery calcium score; CAD, coronary artery disease.



Figure 3 Correlation heatmap of the features used. The numbers represent the Spearman correlation coefficients between the two features. SMS, summed motion score; SRS, summed rest score; HPL, hyperlipidemia; HTN, hypertension; CACS, coronary artery calcium score.

group were 0.896 (95% CI: 0.817–0.975), 0.911 (95% CI: 0.846–0.976), 0.888 (95% CI: 0.802–0.974), 0.899 (95% CI: 0.832–0.965), 0.866 (95% CI: 0.768–0.964), 0.859 (95% CI: 0.768–0.950), 0.874 (95% CI: 0.784–0.964), and 0.845 (95% CI: 0.754–0.937), respectively (Figure 4). The AUC of Rpart was the highest (0.911). In the test group, Rpart and Naïve Bayes had the highest accuracy (0.840). The sensitivity and specificity of Rpart were 0.851 and 0.821, respectively. The sensitivity and specificity of Naïve Bayes were 0.809 and 0.893, respectively. The algorithm with the next highest accuracy was Logistic, with an accuracy of 0.827, a sensitivity of 0.872, and a specificity of 0.750. A high accuracy of 0.813 was also demonstrated by the random forest and XGBoost algorithms. Figure 6 shows the importance of features in the random forest, XGBoost, Logistic, and Rpart algorithms.

Discussion

This study demonstrated the role of ML in detecting obstructive CAD with rest-only MPI combined with CACS

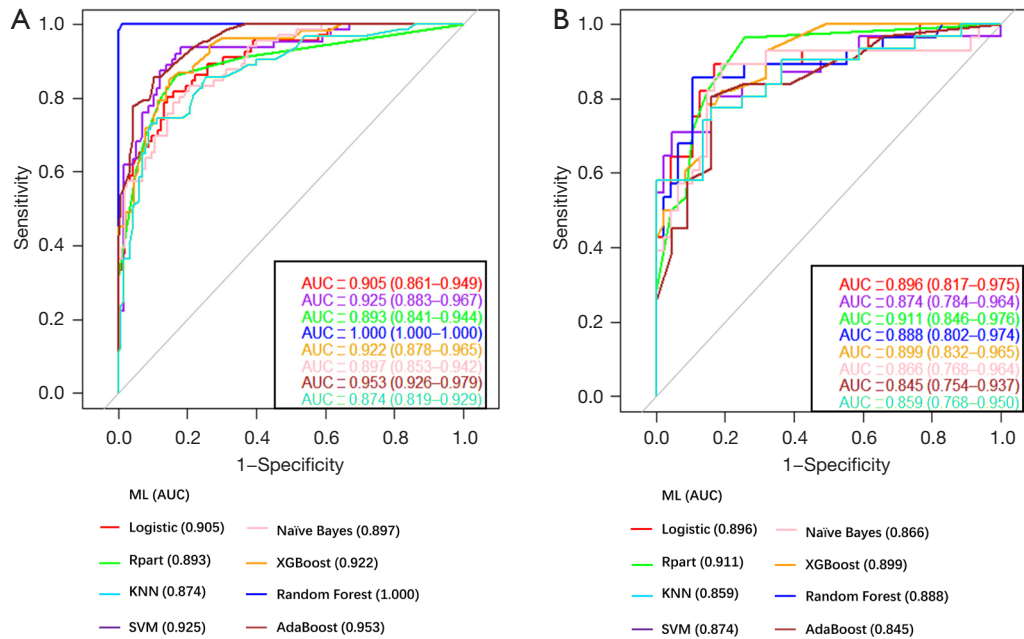


Figure 4 Comparison of ROC curves of 8 ML algorithms. (A) ML performance in the training group. (B) ML performance in the test group. ROC, receiver operator characteristic curve; ML, machine learning; AUC, the area under the receiver operator characteristic curve; KNN, K-nearest neighbor; SVM, support vector machine. Rpart, recursive partitioning and regression trees; XGBoost, extreme gradient boosting; AdaBoost, adaptive boosting.

Table 3 Diagnostic performance of eight ML techniques in the training and test groups

ML techniques	Training group (n=178)					Test group (n=75)				
	Accuracy	Sensitivity	Specificity	PPV	NPV	Accuracy	Sensitivity	Specificity	PPV	NPV
Logistic	0.837	0.857	0.803	0.881	0.768	0.827	0.872	0.750	0.854	0.778
Rpart	0.843	0.830	0.864	0.912	0.750	0.840	0.851	0.821	0.889	0.767
Random forest	0.994	0.991	1.000	1.000	0.985	0.813	0.894	0.679	0.824	0.792
XGBoost	0.850	0.851	0.849	0.902	0.776	0.813	0.851	0.750	0.851	0.750
Naïve Bayes	0.809	0.795	0.833	0.890	0.705	0.840	0.809	0.893	0.927	0.735
KNN	0.843	0.904	0.730	0.860	0.807	0.760	0.864	0.613	0.760	0.760
SVM	0.865	0.835	0.921	0.951	0.753	0.773	0.750	0.807	0.846	0.694
AdaBoost	0.882	0.896	0.857	0.920	0.818	0.787	0.750	0.839	0.868	0.703

ML, machine learning; PPV, positive predictive value; NPV, negative predictive value; Rpart, recursive partitioning and regression trees; KNN, K-nearest neighbor; SVM, support vector machine; XGBoost, extreme gradient boosting; AdaBoost, adaptive boosting.

and cardiovascular risk factors. In the training group, the AUC of random forest was the highest, and the AUCs of Logistic, XGBoost, SVM, and AdaBoost were all above 0.9. In the test group, the AUC of Rpart was the highest (0.911). Rpart and Naïve Bayes had the highest accuracy (0.840). The algorithm with the next highest accuracy was Logistic,

with an accuracy of 0.827, a sensitivity of 0.872, and a specificity of 0.750. This present study demonstrated that combining CACS and cardiovascular risk factors using ML algorithms can improve the performance of resting-gated SPECT MPI for detecting obstructive CAD.

The most common cause of CAD is coronary artery

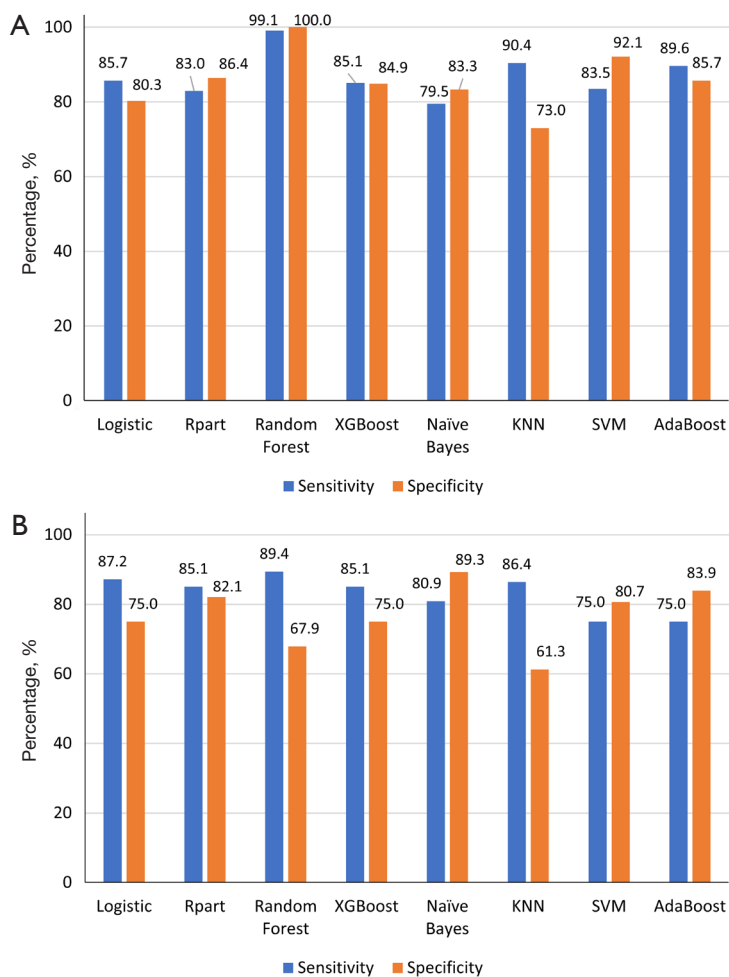


Figure 5 Diagnostic performance of 8 ML algorithms. (A) The sensitivity and specificity of ML algorithms in the training group. (B) The sensitivity and specificity of ML algorithms in the test group. ML, machine learning; KNN, K-nearest neighbor; SVM, support vector machine; Rpart, recursive partitioning and regression trees; XGBoost, extreme gradient boosting; AdaBoost, adaptive boosting.

stenosis due to coronary atherosclerotic plaque. As the degree of stenosis increases, the risk of myocardial ischemia also increases, with myocardial ischemia reaching more than 80% in over 70% of stenotic coronary arteries (34). Gated SPECT MPI is a widely used, well-validated, noninvasive method for detecting myocardial ischemia and obstructive CAD (5,15,35). The value of stress SPECT MPI in the diagnosis and risk stratification of CAD has been widely confirmed (36). Usually, if the SRS is high and obstructive CAD exists, it is myocardial infarction. If the SRS is high yet there is no obstructive CAD, it is pseudo-positive by artifacts. If the SRS is low and there is no obstructive CAD, it is true normal. If the SRS is low and obstructive CAD is present, it is demand ischemia, which is difficult to detect without conventional stress MPI. A previous study found

that the combination of CACS on the basis of stress MPI improved the sensitivity for detecting CAD from 76% to 86%, with no significant difference in specificity (11). However, many patients can still only choose resting MPI due to the contraindication of stress, such as ACS. In addition, rest-only MPI is less effective for detecting CAD, with a sensitivity of approximately 30% (20). Improving the ability of rest-only MPI to diagnose CAD is an urgent clinical issue, and ML is increasingly used in cardiovascular imaging. The present study demonstrated that the combination of resting MPI, CACS, and cardiovascular risk factors improved the diagnosis of obstructive CAD by using ML algorithms. We showed the importance of features in 4 algorithms in the test set. Overall, the importance of SRS was relatively low among the 4 algorithms. A possible reason

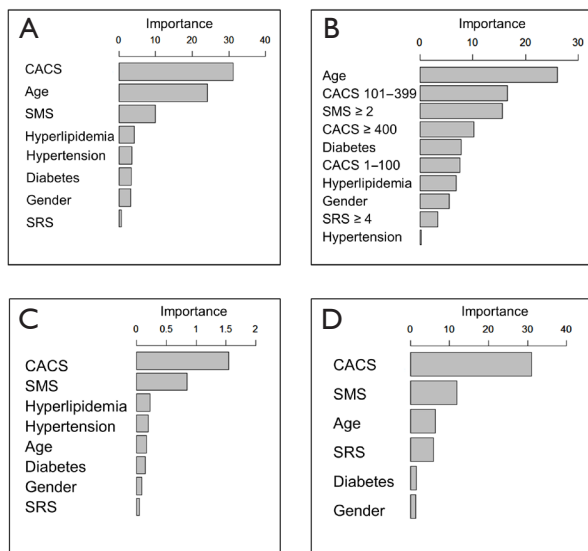


Figure 6 Importance of features for different algorithms. (A) Importance of features for the random forest. (B) Importance of features for the XGBoost. (C) Importance of features for the Logistic. (D) Importance of features for the Rpart. SMS, summed motion score; CACS, coronary artery calcium score; SRS, summed rest score; XGBoost, extreme gradient boosting; Rpart, recursive partitioning and regression trees.

for this might have been that, at rest, even if the coronary arteries significantly narrowed, the myocardial blood flow could still be normal due to coronary compensation. Meanwhile, a previous study confirmed that the sensitivity of rest-only perfusion abnormalities for diagnosing CAD was low (20). Therefore, we believe that SRS still plays a role in different algorithms.

Eight ML algorithms were used in this research. Rpart, Naïve Bayes, XGBoost, Logistic, and random forest were highly accurate for diagnosing obstructive CAD in the test group. Rpart is a decision tree algorithm that operates by recursively dividing the dataset into 2 parts. The features that best reduce the heterogeneity of the outcome variables are taken into account to determine the partition at each stage (37). XGBoost, a scalable end-to-end tree boosting technique, uses a weighted quantile sketch for approximate tree learning and a sparse-aware algorithm for sparse data (38). The Logistic algorithm used in this study is a part of generalized linear models (17). This classifier is widely used in clinical statistical analysis for dichotomous and multicategory outcome variables. The predictor variables and the log odds of the event were supposed to have a linear

relationship by the equation. ADA is a classification tree that fits various stochastic boosting models using adaptive algorithms. A combination of this algorithm and other learning procedures can be used to enhance performance. The output of these procedures, known as weak learners, is merged into a weighted sum that reflects the boosted classifier's final output (39). AdaBoost is a classifier that works similarly to ADA, but is not the same as ADA. Freund and Schapire implemented the M1 algorithm (40). Based on the Statistical Learning Theory, SVM is a powerful supervised ML model for binary and nonlinear classification issues (41). In this study, the sensitivity and specificity in the training set were calculated according to the optimal cutoff value found by Youden's rule, and then the cutoff value was used in the test set to evaluate the sensitivity and specificity. The sensitivity and specificity of the 8 ML methods in the test set were inconsistent, showing different advantages. We used a 10-fold cross-validation approach for the training data (42-45). Ten-fold cross-validation divides the training set into 10 subsamples; 1 single subsample is retained as the data to validate the model, and the other 9 samples are used for training. Therefore, cross-validation can use more sample information to tune hyperparameters.

Computed tomography angiography (CTA) and SPECT MPI, according to the latest European Society of Cardiology (ESC) guidelines (46), are both class I recommendations for suspected CAD patients. CTA is an option for patients with contraindications to stress MPI. A previous study found that CTA had a sensitivity and specificity of 82% and 92%, respectively, for diagnosing ACS in patients with low-risk chest pain (47). The development of ML in CTA further expands its application (48). In this study, resting MPI combined with CACS and cardiovascular risk factors were over 80% accurate in diagnosing obstructive CAD based on the Logistic, Rpart, Naïve Bayes, XGBoost, and random forest algorithms. However, for patients with extensive coronary calcification, arrhythmia, severe obesity, and difficulty holding their breath, CTA may not be appropriate since the image quality will be compromised. Additionally, CTA can provide anatomical stenosis, whereas SPECT MPI combined with CACS can provide anatomical and functional information simultaneously. Our results show that ML can effectively improve the diagnosis of obstructive CAD by rest-only MPI and may be used for CAD screening, although there are still many limitations. ML and AI may be the direction of future development and deserve attention.

Several limitations of this study should be taken into

account. First, this study was not externally validated, and its extrapolation still needs to be validated. Second, patients with stress-related contraindications did not undergo CTA, so it was impossible to compare their diagnostic efficacy. Third, we could not analyze subgroups due to size limitations in the included population, which included multiple contraindications to stress. This study also had a small sample size and needs to be carried out again in a prospective, large sample, multicenter study to validate its findings.

Conclusions

Rest-only SPECT MPI combined with CACS and cardiovascular risk factors using ML algorithms to diagnose obstructive CAD is feasible. Among the algorithms tested in the test group, Rpart, Naïve Bayes, XGBoost, Logistic, and random forest are highly accurate for diagnosing obstructive CAD. The application of ML in resting MPI and CACS may be used for screening obstructive CAD.

Acknowledgments

Funding: This research was partially supported by the National Natural Science Foundation of China (No. 81871381; PI: Yuetao Wang); the Key Laboratory of Changzhou High-tech Research Project (No. CM20193010; PI: Yuetao Wang); the Chinese National Natural Science Foundation for Young Scholars (No. 81901777; PI: Feifei Zhang); and the Science and Technology Project for Youth Talents of Changzhou Health Committee (No. QN201920; PI: Feifei Zhang).

Footnote

Reporting Checklist: The authors have completed the TRIPOD reporting checklist. Available at <https://qims.amegroups.com/article/view/10.21037/qims-22-758/rc>

Conflicts of Interest: All authors have completed the ICMJE uniform disclosure form (available at <https://qims.amegroups.com/article/view/10.21037/qims-22-758/coif>). The authors have no other conflicts of interest to declare.

Ethical Statement: The authors are accountable for all aspects of the work in ensuring that questions related to the accuracy or integrity of any part of the work are appropriately investigated and resolved. The study was

conducted in accordance with the Declaration of Helsinki (as revised in 2013). The Ethics Committee of the Third Affiliated Hospital of Soochow University approved the study protocol, and the requirement for informed consent was waived since the study was retrospective.

Open Access Statement: This is an Open Access article distributed in accordance with the Creative Commons Attribution-NonCommercial-NoDerivs 4.0 International License (CC BY-NC-ND 4.0), which permits the non-commercial replication and distribution of the article with the strict proviso that no changes or edits are made and the original work is properly cited (including links to both the formal publication through the relevant DOI and the license). See: <https://creativecommons.org/licenses/by-nc-nd/4.0/>.

References

1. Klocke FJ, Baird MG, Lorell BH, Bateman TM, Messer JV, Berman DS, et al. ACC/AHA/ASNC guidelines for the clinical use of cardiac radionuclide imaging--executive summary: a report of the American College of Cardiology/American Heart Association Task Force on Practice Guidelines (ACC/AHA/ASNC Committee to Revise the 1995 Guidelines for the Clinical Use of Cardiac Radionuclide Imaging). *Circulation* 2003;108:1404-1418.
2. Sharir T, Ben-Haim S, Merzon K, Prochorov V, Dickman D, Ben-Haim S, Berman DS. High-Speed Myocardial Perfusion Imaging: Initial Clinical Comparison With Conventional Dual Detector Anger Camera Imaging. *JACC Cardiovascular imaging* 2008;1:156-163.
3. Germano G, Kiat H, Kavanagh PB, Moniel M, Mazzanti M, Su H-T, Van Train KE, Berman DS. Automatic quantification of ejection fraction from gated myocardial perfusion SPECT. *J Nucl Med* 1995;36:2138-2147.
4. Chua T, Kiat H, Germano G, Maurer G, Train KV, Friedman J, Berman D. Gated technetium-99m sestamibi for simultaneous assessment of stress myocardial perfusion, postexercise regional ventricular function and myocardial viability: Correlation with echocardiography and rest thallium-201 scintigraphy. *J Am Coll Cardiol* 1994;23:1107-1114.
5. Bavelaar-Croon CDL, Pauwels EKJ, van der Wall EE. Gated single-photon emission computed tomographic myocardial imaging: A new tool in clinical cardiology. *Am Heart J* 2001;141:383-390.
6. Lima RSL, Watson DD, Goode AR, Siadaty MS, Ragosta M, Beller GA, Samady H. Incremental value of combined

- perfusion and function over perfusion alone by gated SPECT myocardial perfusion imaging for detection of severe three-vessel coronary artery disease. *J Am Coll Cardiol* 2003;42:64-70.
7. Berman DS, Kang X, Slomka PJ, Gerlach J, Yang LD, Hayes SW, Friedman JD, Thomson LEJ, Germano G. Underestimation of extent of ischemia by gated SPECT myocardial perfusion imaging in patients with left main coronary artery disease. *J Nucl Cardiol* 2007;14:521-528.
 8. Aziz EF, Javed F, Alviar CL, Herzog E. Triple vessel coronary artery disease presenting as a markedly positive stress electrocardiographic test and a negative SPECT-TL scintigram: a case of balanced ischemia. *Heart Int* 2011;6:e22.
 9. Greenland P, Bonow RO, Brundage BH, Budoff MJ, Eisenberg MJ, Grundy SM, Lauer MS, Post WS, Raggi P, Redberg RF, Rodgers GP, Shaw LJ, Taylor AJ, Weintraub WS. ACCF/AHA 2007 clinical expert consensus document on coronary artery calcium scoring by computed tomography in global cardiovascular risk assessment and in evaluation of patients with chest pain: a report of the American College of Cardiology Foundation Clinical Expert Consensus Task Force (ACCF/AHA Writing Committee to Update the 2000 Expert Consensus Document on Electron Beam Computed Tomography) developed in collaboration with the Society of Atherosclerosis Imaging and Prevention and the Society of Cardiovascular Computed Tomography. *J Am Coll Cardiol* 2007;49:378-402.
 10. Haberl R, Becker A, Leber A, Knez A, Becker C, Lang C, Brüning R, Reiser M, Steinbeck G. Correlation of coronary calcification and angiographically documented stenoses in patients with suspected coronary artery disease: results of 1,764 patients. *J Am Coll Cardiol* 2001;37:451-457.
 11. Schepis T, Gaemperli O, Koepfli P, Namdar M, Valenta I, Scheffel H, Leschka S, Husmann L, Eberli FR, Luscher TF, Alkadhi H, Kaufmann PA. Added value of coronary artery calcium score as an adjunct to gated SPECT for the evaluation of coronary artery disease in an intermediate-risk population. *J Nucl Med* 2007;48:1424-1430.
 12. Arsanjani R, Dey D, Khachatryan T, Shalev A, Hayes SW, Fish M, Nakanishi R, Germano G, Berman DS, Slomka P. Prediction of revascularization after myocardial perfusion SPECT by machine learning in a large population. *J Nucl Cardiol* 2015;22:877-884.
 13. Hu LH, Betancur J, Sharir T, Einstein AJ, Bokhari S, Fish MB, et al. Machine learning predicts per-vessel early coronary revascularization after fast myocardial perfusion SPECT: results from multicentre REFINE SPECT registry. *Eur Heart J Cardiovasc Imaging* 2020;21:549-559.
 14. Juarez-Orozco LE, Martinez-Manzanera O, van der Zant FM, Knol RJJ, Knuuti J. Deep Learning in Quantitative PET Myocardial Perfusion Imaging: A Study on Cardiovascular Event Prediction. *JACC Cardiovasc Imaging* 2020;13:180-182.
 15. Betancur J, Hu LH, Commandeur F, Sharir T, Einstein AJ, Fish MB, Ruddy TD, Kaufmann PA, Sinusas AJ, Miller EJ, Bateman TM, Dorbala S, Di Carli M, Germano G, Otaki Y, Liang JX, Tamarappoo BK, Dey D, Berman DS, Slomka PJ. Deep Learning Analysis of Upright-Supine High-Efficiency SPECT Myocardial Perfusion Imaging for Prediction of Obstructive Coronary Artery Disease: A Multicenter Study. *J Nucl Med* 2019;60:664-670.
 16. Betancur J, Commandeur F, Motlagh M, Sharir T, Einstein AJ, Bokhari S, Fish MB, Ruddy TD, Kaufmann P, Sinusas AJ, Miller EJ, Bateman TM, Dorbala S, Di Carli M, Germano G, Otaki Y, Tamarappoo BK, Dey D, Berman DS, Slomka PJ. Deep Learning for Prediction of Obstructive Disease From Fast Myocardial Perfusion SPECT: A Multicenter Study. *JACC Cardiovasc Imaging* 2018;11:1654-1663.
 17. Megna R, Petretta M, Assante R, Zampella E, Nappi C, Gaudieri V, Mannarino T, D'Antonio A, Green R, Cantoni V, Arumugam P, Acampa W, Cuocolo A. A Comparison among Different Machine Learning Pretest Approaches to Predict Stress-Induced Ischemia at PET/CT Myocardial Perfusion Imaging. *Comput Math Methods Med* 2021;2021:3551756.
 18. Otaki Y, Singh A, Kavanagh P, Miller RJH, Parekh T, Tamarappoo BK, et al. Clinical Deployment of Explainable Artificial Intelligence of SPECT for Diagnosis of Coronary Artery Disease. *JACC Cardiovasc Imaging* 2022;15:1091-1102.
 19. Henzlova MJ, Duvall WL, Einstein AJ, Travin MI, Verberne HJ. ASNC imaging guidelines for SPECT nuclear cardiology procedures: Stress, protocols, and tracers. *J Nucl Cardiol* 2016;23:606-639.
 20. Taban Sadeghi M, Mahmoudian B, Ghaffari S, Moharamzadeh P, Ala A, Pourafkari L, Gureishi S, Roshanravan N, Abolhasani S, Pouraghaei M. Value of early rest myocardial perfusion imaging with SPECT in patients with chest pain and non-diagnostic ECG in emergency department. *Int J Cardiovasc Imaging* 2019;35:965-971.
 21. Liu B, Yu W, Wang J, Shao X, Zhang F, Yang M,

- Yang X, Wu Z, Li S, Shi Y, Wang B, Xu Y, Wang Y. Incremental value of regional wall motion abnormalities for detecting obstructive coronary artery disease by rest-only electrocardiogram-gated single-photon emission computerized tomography myocardial perfusion imaging in suspected coronary artery disease patients. *Nucl Med Commun* 2021;42:276-283.
22. Liu B, Yu W, Wang J, Shao X, Zhang F, Zhou M, Shi Y, Wang B, Xu Y, Wang Y. A model combining rest-only ECG-gated SPECT myocardial perfusion imaging and cardiovascular risk factors can effectively predict obstructive coronary artery disease. *BMC Cardiovasc Disord* 2022;22:268.
 23. Dorbala S, Ananthasubramaniam K, Armstrong IS, Chareonthaitawee P, DePuey EG, Einstein AJ, Gropler RJ, Holly TA, Mahmarian JJ, Park MA, Polk DM, Russell R, 3rd, Slomka PJ, Thompson RC, Wells RG. Single Photon Emission Computed Tomography (SPECT) Myocardial Perfusion Imaging Guidelines: Instrumentation, Acquisition, Processing, and Interpretation. *J Nucl Cardiol* 2018;25:1784-1846.
 24. Cerqueira MD, Weissman NJ, Dilsizian V, Jacobs AK, Kaul S, Laskey WK, Pennell DJ, Rumberger JA, Ryan T, Verani MS. Standardized myocardial segmentation and nomenclature for tomographic imaging of the heart: A statement for healthcare professionals from the Cardiac Imaging Committee of the Council on Clinical Cardiology of the American Heart Association. *Circulation* 2002;105:539-542.
 25. Sharir T, Berman DS, Waechter PB, Areeda J, Kavanagh PB, Gerlach J, Kang X, Germano G. Quantitative analysis of regional motion and thickening by gated myocardial perfusion SPECT: Normal heterogeneity and criteria for abnormality. *J Nucl Med* 2001;42:1630-1638.
 26. Sharir T, Germano G, Waechter PB, Kavanagh PB, Areeda JS, Gerlach J, Kang X, Lewin HC, Berman DS. A new algorithm for the quantitation of myocardial perfusion SPECT. II: validation and diagnostic yield. *J Nucl Med* 2000;41:720-727.
 27. Agatston AS, Janowitz WR, Hildner FJ, Zusmer NR, Viamonte M, Jr., Detrano R. Quantification of coronary artery calcium using ultrafast computed tomography. *J Am Coll Cardiol* 1990;15:827-832.
 28. Go AS, Mozaffarian D, Roger VL, Benjamin EJ, Berry JD, Bhalra MJ, et al. Heart disease and stroke statistics--2014 update: a report from the American Heart Association. *Circulation* 2014;129:e28-e292.
 29. Arad Y, Goodman KJ, Roth M, Newstein D, Guerci AD. Coronary calcification, coronary disease risk factors, C-reactive protein, and atherosclerotic cardiovascular disease events: the St. Francis Heart Study. *J Am Coll Cardiol* 2005;46:158-165.
 30. Karimi-Ashtiani S, Arsanjani R, Fish M, Kavanagh P, Germano G, Berman D, Slomka P. Direct quantification of left ventricular motion and thickening changes using rest-stress myocardial perfusion SPECT. *J Nucl Med* 2012;53:1392-1400.
 31. Friedman J, Hastie T, Tibshirani R. Regularization Paths for Generalized Linear Models via Coordinate Descent. *J Stat Softw* 2010;33:1-22.
 32. Liaw A, Wiener M. Classification and Regression by randomForest. *R News* 2002;2:18-22.
 33. Alfaro E, Gamez M. An R Package for Classification with Boosting and Bagging. *J Stat Softw* 2013;52:1-35.
 34. Tonino PA, Fearon WF, De Bruyne B, Oldroyd KG, Leeser MA, Ver Lee PN, Maccarthy PA, Van't Veer M, Pijls NH. Angiographic versus functional severity of coronary artery stenoses in the FAME study fractional flow reserve versus angiography in multivessel evaluation. *J Am Coll Cardiol* 2010;55:2816-2821.
 35. Betancur J, Otaki Y, Motwani M, Fish MB, Lemley M, Dey D, Gransar H, Tamarappoo B, Germano G, Sharir T, Berman DS, Slomka PJ. Prognostic Value of Combined Clinical and Myocardial Perfusion Imaging Data Using Machine Learning. *JACC Cardiovasc Imaging* 2018;11:1000-1009.
 36. Fihn SD, Gardin JM, Abrams J, Berra K, Blankenship JC, Dallas AP, et al. 2012 ACCF/AHA/ACP/AATS/PCNA/SCAI/STS guideline for the diagnosis and management of patients with stable ischemic heart disease: a report of the American College of Cardiology Foundation/American Heart Association task force on practice guidelines, and the American College of Physicians, American Association for Thoracic Surgery, Preventive Cardiovascular Nurses Association, Society for Cardiovascular Angiography and Interventions, and Society of Thoracic Surgeons. *Circulation* 2012;126:e354-471.
 37. Speybroeck N. Classification and regression trees. *Int J Public Health* 2012;57:243-246.
 38. Hou N, Li M, He L, Xie B, Wang L, Zhang R, Yu Y, Sun X, Pan Z, Wang K. Predicting 30-days mortality for MIMIC-III patients with sepsis-3: a machine learning approach using XGboost. *J Transl Med* 2020;18:462.
 39. Dou L, Li X, Zhang L, Xiang H, Xu L. iGlu_AdaBoost: Identification of Lysine Glutarylation Using the AdaBoost Classifier. *J Proteome Res* 2021;20:191-201.

40. Freund Y, Schapire RE. Experiments with a new boosting algorithm. in Proceedings of the Thirteenth International Conference on Machine Learning 1996;pp.148–156.
41. Yang Q, Zhang H, Xia J, Zhang X. Evaluation of magnetic resonance image segmentation in brain low-grade gliomas using support vector machine and convolutional neural network. *Quant Imaging Med Surg* 2021;11:300-316.
42. de Souza Filho EM, Fernandes FA, Wiefels C, de Carvalho LND, Dos Santos TF, Dos Santos A, Mesquita ET, Seixas FL, Chow BJW, Mesquita CT, Gismondi RA. Machine Learning Algorithms to Distinguish Myocardial Perfusion SPECT Polar Maps. *Front Cardiovasc Med* 2021;8:741667.
43. de Souza Filho EM, Fernandes FA, Portela MGR, Newlands PH, de Carvalho LND, Dos Santos TF, Dos Santos A, Mesquita ET, Seixas FL, Mesquita CT, Gismondi RA. Machine Learning Algorithms to Detect Sex in Myocardial Perfusion Imaging. *Front Cardiovasc Med* 2021;8:741679.
44. Ou X, Zhang J, Wang J, Pang F, Wang Y, Wei X, Ma X. Radiomics based on (18) F-FDG PET/CT could differentiate breast carcinoma from breast lymphoma using machine-learning approach: A preliminary study. *Cancer Med* 2020;9:496-506.
45. Shu ZY, Cui SJ, Zhang YQ, Xu YY, Hung SC, Fu LP, Pang PP, Gong XY, Jin QY. Predicting Chronic Myocardial Ischemia Using CCTA-Based Radiomics Machine Learning Nomogram. *J Nucl Cardiol* 2022;29:262-274.
46. Knuuti J, Wijns W, Saraste A, Capodanno D, Barbato E, Funck-Brentano C, et al. 2019 ESC Guidelines for the diagnosis and management of chronic coronary syndromes. *Eur Heart J* 2020;41:407-477.
47. Gallagher MJ, Ross MA, Raff GL, Goldstein JA, O'Neill WW, O'Neil B. The diagnostic accuracy of 64-slice computed tomography coronary angiography compared with stress nuclear imaging in emergency department low-risk chest pain patients. *Ann Emerg Med* 2007;49:125-136.
48. Benjamin MM, Rabbat MG. Machine learning-based advances in coronary computed tomography angiography. *Quant Imaging Med Surg* 2021;11:2208-2213.

Cite this article as: Liu B, Yu W, Zhang F, Shi Y, Yang L, Jiang Q, Wang Y, Wang Y. Detecting obstructive coronary artery disease with machine learning: rest-only gated single photon emission computed tomography myocardial perfusion imaging combined with coronary artery calcium score and cardiovascular risk factors. *Quant Imaging Med Surg* 2023;13(3):1524-1536. doi: 10.21037/qims-22-758